# Gold(III) porphyrins: Synthesis and interaction with G-quadruplex DNA

Tiffany Rundstadler, Emmanuelle Mothes, Samir Amrane, Jean-Luc Stigliani, Pierre Verhaeghe, G. Pratviel

# Gold(III) porphyrins: synthesis and interaction with G-quadruplex DNA

Tiffany Rundstadler,[a,b] Emmanuelle Mothes,[a,b] Samir Amrane,[c,d] Jean-Luc Stigliani,[a,b] Pierre Verhaeghe,[a,b] Geneviève Pratviel[a,b,*]

[a] *Laboratoire de Chimie de Coordination, LCC, CNRS, Toulouse, France*

[b] *Université de Toulouse, UPS, Toulouse, France*

[c] *Université de Bordeaux, Bordeaux, France*

[d] *ARNA Laboratory, INSERM U1212, CNRS UMR 5320, IECB, Bordeaux, France*

* Corresponding author at: LCC-CNRS, 205 route de Narbonne, 31077 Toulouse cedex4, France. E-mail address: genevieve.pratviel@lcc-toulouse.fr

**Abstract**

G-quadruplex nucleic acids (G4s) are RNA and DNA secondary structures involved in the regulation of multiple key biological processes. They can be found in telomeres, oncogene promoters, RNAs, but also in viral genomes. Due to their unique structural features, very distinct from the canonical duplexes or single-strands, G4s represent promising pharmacological targets for small molecules, namely G4-ligands. Gold(III) penta-cationic porphyrins, as specific G4 ligands, are able to inhibit HIV-1 infectivity and their antiviral activity correlates with their affinity for G4s. Up to now, one of the best antiviral compounds is *meso*-5,10,15,20-tetrakis[4-(*N*-methyl-pyridinium-2-yl)phenyl]porphyrinato gold(III) (**1**). Starting from this compound, we report a structure/affinity relationship study of gold(III) cationic porphyrins to find out the best porphyrin candidate for functionalization, in order to study the antiviral mechanism of action of these gold(III) porphyrins.

**Key-words**

$Au^{3+}$-complexes, FRET melting, HIV-1, cationic porphyrins, modeling, G4

## 1. Introduction

G-quadruplex nucleic acids (also referred to as G4s) are unusual secondary DNA and RNA structures formed in guanine-rich sequences. G4 forming sequences include several consecutive rows of guanines, which are separated by single-stranded sequences composed of 1 to 15 nucleotides. Four guanines associate in planar G-quartets. Two, three or more G-quartets can stack on top of each other.

The stability of the structure is due to Hoogsteen-type hydrogen bonds between guanines within one quartet, coordination of $K^+$ (and/or $Na^+$) monovalent cations and π-π stacking between successive G-quartets. G4s may show various strand orientations and stoichiometry, various loop types and size [1, 2].

The formation of G4s *in vivo* is well documented [3, 4]. Besides, G4s, as unique nucleic acid 3D structures, were shown to be associated to the regulation of numerous key biological processes such as telomere maintenance, replication, transcription, RNA splicing and translation [5-9] including involvement in the viruses replication cycles [10-13].

Progresses in the structural characterization of G4s and in the identification of their involvement in some diseases such as cancer [14, 15] or others [5, 16, 17] led to massive efforts toward the synthesis of G4-ligands[18-24]. Some G4-ligands indeed showed biological activity, among which antiviral properties is an emerging field [10, 25-28].

Due to their large aromatic structure and cationic character, cationic porphyrins are powerful G4-ligands. They bind to G4s by electrostatic and external π-stacking interactions [29, 30]. In addition to the most studied porphyrin, *meso*-5,10,15,20-tetrakis(*N*-methylpyridinium-4-yl)porphyrin, TMPyP4 [31], second-generation of cationic porphyrin derivatives with better affinity and selectivity toward G-quadruplex DNA were reported [32-37]. Some of them exhibit significant antiviral properties against HIV-1 [38], in particular porphyrin **1** (Scheme 1) [38, 39]. The antiviral activity of cationic porphyrins correlates with their capacity to bind G-quadruplex DNA [38]. Several G4s were found in the U3 region of the long terminal repeat sequence (LTR) of HIV-1, located at both ends of the proviral DNA genome. In the 5'-LTR, the U3-G4 sequences overlap with the binding sites of SP1 transcription factor in the promoter of the viral genome [40-42]. The presence of G4-forming sequences in the GAG [43] and the POL [44, 45] genes of HIV-1 were also reported. Nevertheless, whether these G4s might actually correspond to antiviral pharmacological targets of antiviral cationic porphyrins remains to be fully demonstrated.

In the present work, we describe the preparation of gold(III) porphyrin derivatives, based on modifications of porphyrin **1**, with various numbers of charges and different charge locations. We measure their affinity and selectivity for G-quadruplex DNA through fluorescence-based Förster resonance energy transfer (FRET)-melting assay. We observe that, in the present new series of bulky cationic porphyrins (and as previously observed for other series of cationic porphyrins) [33, 46-50], the number of positive charges is crucial for affinity. The decrease of G4-binding affinity with the reduction of the number of charges is significant. Moreover, the location of the charges is also important. This structure/activity relationship allowed us to select the best porphyrin candidate for functionalization in view of further studies on the mechanism of action of the promising anti-HIV porphyrin **1**.

## 2. Experimental

### *2.1. Chemicals and reagents*

Oligonucleotides were purchased from Eurogentec (Belgium). All commercially available compounds were purchased from Aldrich and/or Fluorochem. Sep-Pak C18 5 g columns were purchased from Waters. Dowex 1x8-200 (chloride form) resin was purchased from Aldrich. $^1$H-NMR spectra were recorded on Bruker Avance Neo 600, 400 and/or 300 spectrometer using the residual solvent peak as internal calibration. Mass spectra were recorded either on a QTof premier HAB262 (electrospray) or Xevo G2 QTOF (high resolution electrospray). UV-vis spectra were recorded on a Hewlett Packard 8452A spectrophotometer.

### *2.2. Synthesis of gold(III) porphyrins*

#### *2.2.1. Preparation of meso-5-(4-bromophenyl)-10,15,20-tris[4-(N-methyl-pyridinium-2-yl)phenyl]porphyrinato gold(III) tetrachloride (**2**) and meso-5,15-bis(4-bromophenyl)-10,20-bis[4-(N-methyl-pyridinium-2-yl)phenyl]porphyrinato gold(III) trichloride (**3**)*

*2.2.1.1. Preparation of 4-(2-pyridinyl)dipyrromethane*, adapted from [51]

Freshly distilled pyrrole (30.4 mL, 440 mmol, 20 equiv.) and 4-(2-pyridinyl)benzaldehyde (4 g, 21.8 mmol) were mixed and purged with argon in the dark for 15 min. Trifluoroacetic acid (0.2 mL, 2.6 mmol) was added under argon and the mixture was stirred for 20 h in the dark at RT. At the end of the reaction, the excess pyrrole was removed *in vacuo*. The residue was purified by column chromatography on silica with $CH_2Cl_2$/ethyl acetate as eluent (ethyl acetate gradient from 0 to 15%). After evaporation of the collected fraction, the product was dissolved in $CH_2Cl_2$ and precipitated with petroleum ether to afford dipyrromethane as off-white solid. Yield 3.5 g, 56%. TLC ($SiO_2$, $CH_2Cl_2$/AcOEt, 4/1), Rf: 0.58. $^1$H NMR (400 MHz, $CDCl_3$, $\delta$ ppm): 8.66 (d, *J* = 4.8 Hz, 1H, pyridine), 8.07 (bs, 2H, NH), 7.92 (d, *J* = 8 Hz, 2H, phenyl), 7.77-7.68 (m, 2H, pyridine), 7.30 (d, *J* = 8 Hz, 2H, phenyl), 7.24-7.21 (m, 1H, pyridine), 6.68 (bs, 2H, pyrrole), 6.18 (d, *J* = 2.9 Hz, 2H, pyrrole), 5.95 (bs, 2H, pyrrole), 5.50 (s, 1H, CH). MS-ES$^+$ (*m/z*): 300.1 $[M+H]^+$.

*2.2.1.2. Preparation of free base porphyrins, meso-5-(4-bromophenyl)-10,15,20-tris[4-(pyridin-2-yl)phenyl]porphyrin (**6**) and meso-5,15-bis(4-bromophenyl)-10,20-bis[4-(pyridin-2-yl)phenyl]porphyrin (**7**)*

4-(2-pyridinyl)dipyrromethane (1 g, 3.3 mmole, 2 equiv.), 4-bromobenzaldehyde (304.6 mg, 1.64 mmole, 1 equiv.), and 4-(2-pyridinyl)benzaldehyde (308.5 mg, 1.68 mole, 1 equiv.) were dissolved in

propionic acid (50 mL) and the mixture was refluxed for 3 h in the dark. Propionic acid was removed by distillation. The dry product was dissolved in $CH_2Cl_2$, mixed with a small quantity of silica, dried *in vacuo*, and purified by silica chromatography. The symmetric *meso*-5,15-bis(4-bromophenyl)-10,20-bis[4-(pyridin-2-yl)phenyl]porphyrin (**7**) was first obtained by elution with 100% dichloromethane. Elution with additional 0.4% methanol afforded the 5-(4-bromophenyl)-10,15,20-tris[4-(pyridin-2-yl)phenyl]porphyrin (**6**). The fractions were evaporated *in vacuo*. The porphyrins were dissolved in $CH_2Cl_2$ and precipitated with petroleum ether (40–60 °C). Yield: porphyrin **6**, purple solid, 240 mg, 16%; porphyrin **7**, purple solid 120 mg, 8%.

Porphyrin (**6**): TLC ($SiO_2$, $CH_2Cl_2$/MeOH, 98/2), Rf: 0.65. $^1$H NMR (400 MHz, $CDCl_3$, $\delta$ ppm): 8.95 (m, 6H, pyrrole), 8.87 – 8.85 (m, 5H, pyridine Hm, pyrrole), 8.40 (d, 6H, *J* = 8 Hz, phenyl Hg), 8.35 – 8.33 (m, 6H, phenyl Hf), 8.10 (d, 2H, *J* = 8 Hz, Br-phenyl Hb), 8.07 – 8.05 (m, 3H, pyridine Hj), 7.95 – 7.90 (m, 5H, Br-phenyl Hc, pyridine Hk), 7.39 – 7.36 (m, 3H, pyridine Hl), -2.74 (s, 2H, NH). $^{13}$C NMR (101 MHz, $CDCl_3$, 323K, $\delta$ ppm): 157.6 (i), 150.2 (m), 143.1 (e), 141.3 (a), 139.2 (h), 137.1 (k), 136.0 (b), 135.2 (f), 131.5 (pyrrole), 130.1 (c), 125.5 (g), 122.5 (l), 121.0 (j), 120.2 (5, 10, 15, 20), 118.5 (d). MS-ES$^+$ (*m/z*): 924.2 (45%) $[M+H]^+$, 926.2 (50%) $[M+H]^+$, 462.6 (80%) $[M+2H]^{2+}$, 463.6 (100%) $[M+2H]^{2+}$. UV-vis ($CHCl_3$, $\lambda$ nm ($\varepsilon$ $M^{-1}$ $cm^{-1}$)): 422 (520 $10^3$), 517 (18.3 $10^3$), 553 (9.9 $10^3$), 591 (4.7 $10^3$), 648 (4 $10^3$).

Porphyrin (**7**): TLC ($SiO_2$, $CH_2Cl_2$/MeOH, 98/2), Rf: 0.83. $^1$H NMR (400 MHz, $CDCl_3$, $\delta$ ppm): 8.95 (d, *J* = 4.5 Hz, 4H, pyrrole), 8.88 – 8.84 (m, 6H, pyridine and pyrrole), 8.40 (d, *J* = 8 Hz, 4H, phenyl), 8.33 (d, *J* = 8 Hz, 4H, phenyl), 8.09 (d, *J* = 8 Hz, 2H, Br-phenyl), 8.07 – 8.05 (m, 2H, pyridine), 7.95 – 7.89 (m, 6H, Br-phenyl, pyridine), 7.40 – 7.37 (m, 2H, pyridine), -2.78 (s, 2H, NH). MS-ES$^+$ (*m/z*): 925.1 (80%) $[M+H]^+$, 927.1 (100%) $[M+H]^+$. UV-vis ($CHCl_3$, $\lambda$ nm ($\varepsilon$ $M^{-1}$ $cm^{-1}$)): 421 (520 $10^3$), 517 (20 $10^3$), 552 (10 $10^3$), 591 (6 $10^3$), 648 (5 $10^3$).

*2.2.1.3. Preparation of methylated free base porphyrin, meso-5-(4-bromophenyl)-10,15,20-tris[4-N-methyl-pyridinium-2-yl)phenyl]porphyrin tristrifluoroacetate (**8**)*

Porphyrin **6** (70 mg, 0.075 mmol) was dissolved in anhydrous dimethyl formamide (DMF) (4 mL) and a large excess of iodomethane (1.5 mL) was added. The mixture was heated at 100 °C for 3 h in the dark. Iodomethane and DMF were removed by *vacuum* distillation. The residue was dissolved in acetonitrile and precipitated with diethyl ether. After centrifugation, the product was dried in vacua. The product was diluted in $H_2O$/$CH_3CN$ (95:5). It was purified on Sep Pak C18 column (5 g), elution $H_2O$ with 0.1% trifluoroacetic acid (TFA), then $H_2O$/$CH_3CN$ (60:40) with 0.1% TFA. The fractions were evaporated *in vacuo*. The dry product was dissolved in methanol and the solvent evaporated *in vacuo*. This step was repeated several times to remove TFA. The last step was a precipitation with diethyl ether. After centrifugation and drying, a purple solid is obtained. Yield: 87 mg, 88%. TLC ($SiO_2$,

$CH_3CN/H_2O/KNO_3$sat., 6/1/1), Rf: 0.5. $^1$H NMR (400 MHz, DMSO-$d_6$, $\delta$ ppm): 9.35 – 9.33 (m, 3H, pyridine), 9.02 (s, 4H, pyrrole), 9.00 (d, *J* = 5 Hz, 2H, pyrrole), 8.96 (d, *J* = 5 Hz, 2H, pyrrole), 8.85 – 8.81 (m, 3H, pyridine), 8.54 (d, *J* = 8 Hz, 2H, phenyl15), 8.53 (d, *J* = 8 Hz, 4H, phenyl10,20), 8.54 – 8.47 (m, 3H, pyridine), 8.34 – 8.30 (m, 3H, pyridine), 8.21 (d, *J* = 8 Hz, 2H, Br-phenyl), 8.18 (d, *J* = 8 Hz, 2H, phenyl15), 8.18 (d, *J* = 8 Hz, 4H, phenyl10,20), 8.07 (d, *J* = 8 Hz, 2H, Br-phenyl), 4.52 (s, 9H, methyl), -2.87 (s, 2H, NH). MS-ES$^+$ (*m/z*): 322.77 (80%) $[M]^{3+}$, 323.44 (100%) $[M]^{3+}$. UV-vis ($H_2O$, $\lambda$ nm ($\varepsilon$ $M^{-1}$ $cm^{-1}$)): 415 (370 $10^3$), 516 (13.8 $10^3$), 554 (6.9 $10^3$), 580 (5.4 $10^3$), 635 (3.2 $10^3$). UV-vis (acidic $H_2O$, $\lambda$ nm): 437, 649.

*2.2.1.4. Preparation of methylated free base porphyrin, meso-5,15-bis(4-bromophenyl)-10,20-bis[4-N-methylpyridinium-2-yl)phenyl]porphyrin bistrifluoroacetate (**9**)*

Porphyrin **7** (75 mg, 0.081 mmol) was dissolved in anhydrous DMF (4 mL) and a large excess of iodomethane (1.5 mL) was added. The mixture was heated at 100 °C for 3 h in the dark. Iodomethane and DMF were removed by *vacuum* distillation. The residue was dissolved in methanol and precipitated with diethyl ether. After centrifugation, the product was dried *in vacuo*. The product was diluted in $H_2O/CH_3CN$ (95:5). It was purified on Sep Pak C18 column (5 g), elution $H_2O$ with 0.1% TFA, then $H_2O/CH_3CN$ (60:40) with 0.1% TFA. The fractions were evaporated. The dry product was dissolved in acetonitrile and precipitated with diethyl ether. After centrifugation and drying, a purple solid is obtained. Yield: 45 mg, 47%. TLC ($SiO_2$, $CH_3CN/H_2O/KNO_3$sat., 6/1/1), Rf: 0.7. $^1$H NMR (400 MHz, DMSO-$d_6$, $\delta$ ppm): 9.32 (dd, *J* = 6 Hz and 1.5 Hz, 2H, pyridine), 8.98 (d, *J* = 4.8 Hz, 4H, pyrrole), 8.94 (d, *J* = 4.8 Hz, 4H, pyrrole), 8.82 (ddd, *J* = 8, 8 and 1.5 Hz, 2H, pyridine), 8.52 (d, *J* = 8.4 Hz, 4H, phenyl), 8.49 (d, *J* = 8 Hz, 2H, pyridine), 8.31 (ddd, *J* = 8, 6, and 1.2 Hz, 2H, pyridine), 8.20 (d, *J* = 8.4 Hz, 4H, Br-phenyl), 8.16 (d, *J* = 8.4 Hz, 4H, phenyl), 8.07 (d, *J* = 8.4 Hz, 4H, Br-phenyl), 4.52 (s, 6H, methyl), -2.91 (s, 2H, NH). MS-ES$^+$ (*m/z*): 477.1 (50%) $[M]^{2+}$, 478.1 (100%) $[M]^{2+}$. UV-vis ($H_2O/CH_3CN$, 50/50, $\lambda$ nm): 416 (160 $10^3$), 513 (6.8 $10^3$), 549 (3 $10^3$), 588 (2 $10^3$), 645 (1.8 $10^3$). UV-vis (acidic $H_2O/CH_3CN$, $\lambda$ nm): 444, 658.

*2.2.1.5. Preparation of gold(III) porphyrin, meso-5-(4-bromophenyl)-10,15,20-tris[4-(N-methyl-pyridinium-2-yl)phenyl]porphyrinato gold(III) tetrachloride (**2**)*

Porphyrin **8** (87 mg, 66.5 µmol) was dissolved in $H_2O$ (40 mL) with $KAuCl_4$ (66.3 mg, 175 µmol, 2.5 equiv.). The reaction medium was refluxed during 20 h. The metallation was followed by the shift of the Soret band of the non-metallated porphyrin from 415 to 437 nm in acid medium. After evaporation of the solvent, the product was purified by reverse phase chromatography on a Sep Pak C18 cartridge (5 g), elution with $H_2O$, 0.1% TFA, then $CH_3CN/H_2O$ (40:60) 0.1% TFA. The fractions containing the gold(III) porphyrin were evaporated, the product was dissolved in acetonitrile and the solvent

evaporated under vacuum several times to eliminate TFA. Finally, the porphyrin was dissolved in acetonitrile and precipitated with diethyl ether. After centrifugation, the pellet was dissolved in 20 mL of $CH_3CN/H_2O$ (50:50). Anion exchange was performed on a dowex 1x8-200 resin column (chloride form, 1 g) during 24 h. The solution was filtered off and evaporated. The product was dissolved in methanol and precipitated with diethyl ether. After centrifugation, the pellet was dried. Yield: red solid, 65 mg, 75%. TLC ($SiO_2$, $CH_3CN/H_2O/KNO_3$sat., 6/1/1), Rf: 0.42. $^1$H NMR (400 MHz, MeOD, $\delta$ ppm): 9.58 (s, 4H, pyrrole), 9.55 (d, *J* = 5.3 Hz, 2H, pyrrole), 9.48 (d, *J* = 5.3 Hz, 2H, pyrrole), 9.25 – 9.23 (m, 3H, pyridine), 8.85 – 8.81 (m, 3H, pyridine), 8.65 (d, *J* = 8 Hz, 2H, phenyl 15), 8.63 (d, *J* = 8 Hz, 4H, phenyl 10, 20), 8.49 – 8.47 (m, 3H, pyridine), 8.29 – 8.24 (m, 11H, pyridine + phenyl, Br-phenyl), 8.14 (d, *J* = 8.4 Hz, 2H, Br-phenyl), 4.64 (s, 3H, methyl 15), 4.63 (s, 6H, methyl 10,20). $^{13}$C NMR (101 MHz, MeOD, $\delta$ppm): 156.4, 147.7, 146.6, 142.6, 138.4, 137.9, 137.7, 137.7, 136.3, 135.5, 133.7, 133.1, 133.1, 131.6, 131.1, 129.3, 129.3, 128.1, 127.9, 124.749, 123.4, 122.9, 122.9. $^{19}$F NMR (376 MHz, DMSO-$d_6$): no signal. HRMS-ES$^+$ (*m/z*): calcd. for $C_{62}H_{45}AuBrN_7$ 290.81460 (and 291.31450), found 290.8140 (and 291.3140) $[M]^{4+}$. UV-vis ($H_2O$, $\lambda$ nm ($\varepsilon$ $M^{-1}$ $cm^{-1}$)): 406 (340 $10^3$), 520 (16 $10^3$).

*2.2.1.6. Preparation of meso-5,15-bis(4-bromophenyl)-10,20-bis[4-(N-methyl-pyridinium-2-yl)phenyl]porphyrinato gold(III) trichloride (**3**)*

Porphyrin **9** (45 mg, 38 µmol) was dissolved in ethanol (5 mL) and $H_2O$ (5 mL) and NaOH (76 µmol, 2 equiv.). $KAuCl_4$ (87 mg, 228 µmol, 6 equiv.) was dissolved in 1 mL $H_2O$ and added to the porphyrin solution. The reaction medium was refluxed during 24 h. The metallation was followed by the shift of the Soret band of the non-metallated porphyrin from 417 to 444 nm in acid medium. The metallation was about 90%. After evaporation of the solvent the product was purified by reverse phase chromatography on a Sep-Pak C18 cartridge (5 g). Elution with $H_2O$, 0.1% TFA, then $CH_3CN/H_2O$ ($CH_3CN$ gradient from 0 to 80%) 0.1% TFA. The fractions containing the gold(III) porphyrin were evaporated, the product was dissolved in acetonitrile and evaporated under vacuum several times to eliminate TFA. Finally, the porphyrin was dissolved in acetonitrile and precipitated with diethyl ether. After centrifugation, the pellet was dissolved in 20 mL of $CH_3CN/H_2O$ (50:50). Anion exchange was performed on a dowex 1x8-200 resin column (chloride form, 1 g) during 24 h. The product solution was evaporated to dryness. The product was dissolved in acetonitrile and precipitated with diethyl ether. After centrifugation, the pellet was dried. Yield: red solid, 26 mg, 54%. TLC ($SiO_2$, $CH_3CN/H_2O/KNO_3$sat., 6/1/1), Rf: 0.65. $^1$H NMR (400 MHz, DMSO-$d_6$, $\delta$ ppm): 9.53 (d, *J* = 5.3 Hz, 4H, pyrrole), 9.47 (d, *J* = 5.3 Hz, 4H, pyrrole), 9.24 (d, *J* = 6 Hz, 2H, pyridine), 8.83 (t, *J* = 7.8 Hz, 2H, pyridine), 8.60 (d, *J* = 8 Hz, 4H, phenyl), 8.47 (d, *J* = 8 Hz, 2H, pyridine), 8.29 – 8.22 (m, 10H, pyridine + Br-phenyl, phenyl), 8.13 (d, *J* = 8 Hz, 4H, Br-phenyl), 4.62 (s, 6H, methyl). $^{13}$C NMR (101 MHz, MeOD, $\delta$ ppm): 156.4, 147.7, 146.6,

142.6, 138.4, 137.8, 137.6, 136.3, 135.5, 133.7, 133.1, 132.9, 131.7, 131.1, 129.2, 127.9, 124.7, 123.3, 122.8. $^{19}$F NMR (376 MHz, DMSO-$d_6$): no signal. HRMS-ES$^+$ (*m/z*): calcd. for $C_{56}H_{38}AuBr_2N_6$ 383.03970 (and 383.70590, 100%), found 383.0396 (and 383.7059 100%) $[M]^{3+}$. UV-vis ($H_2O$, $\lambda$ nm ($\varepsilon$ $M^{-1}$ $cm^{-1}$)): 406 (260 $10^3$), 521 (13 $10^3$).

*2.2.2. Preparation of meso-tetrakis[4-(N-methylpyridinium-4-yl)phenyl]porphyrinato gold(III) pentachloride (**4**)*

*2.2.2.1. Preparation of meso-5,10,15,20-tetrakis[4-(pyrid-4-yl)phenyl]porphyrin (**10**)*

*Meso*-5,10,15,20-tetrakis[4-(pyrid-4-yl)phenyl]porphyrin (**10**) was prepared according to a previously published procedure [33] with some modifications. The 4-(pyrid-2-yl)benzaldehyde (1.50 g, 8.2 mmol) was dissolved in propionic acid (40 mL). Freshly distilled pyrrole (0.58 mL, 8.3 mmol) was added and the mixture was refluxed during 1h 30 min in the dark. The solvent was evaporated, the residue was taken up with DMF and filtered. The precipitate was washed with DMF and diethyl ether and dried under *vacuum*. Yield: purple solid, 263 mg, 14%. Due to the poor solubility of the compound, the characterization was not possible.

*2.2.2.2. Preparation of meso-5,10,15,20-tetrakis[4-(N-methyl-pyridinium-4-yl)phenyl]porphyrin tetraiodide (**11**)*

Porphyrin **10** (166 mg, 0.18 mmol) was methylated by a large excess of iodomethane (3 mL) in DMF (5 mL) at 100 °C during 3 h. The reaction was followed by TLC. Iodomethane and DMF were removed by *vacuum* distillation. The reaction was complete and the crude solid was used without further purification. TLC ($SiO_2$, $CH_3CN/H_2O/KNO_3$sat., 8/1/1), Rf: 0.48. $^1$H NMR (400 MHz, DMSO-$d_6$, $\delta$ ppm): 9.23 (d, 8H, *J* = 7 Hz, pyridine), 8.97 (s, 8H, pyrrole), 8.88 (d, 8H, *J* = 7 Hz, pyridine), 8.59 (d, 8H, *J* = 8.5 Hz, phenyl), 8.53 (d, 8H, *J* = 8.5 Hz, phenyl), 4.47 (s, 12H, methyl), -2.84 (s, 2H, NH). MS-ES$^+$ (*m/z*): 245.6 (80%) $[M]^{4+}$, 322.5 (100%) $[M\text{-}CH_3]^{3+}$.

*2.2.2.3. Preparation of meso-5,10,15,20-tetrakis[4-(N-methyl-pyridinium-4-yl)phenyl]porphyrinato gold(III) pentachloride (**4**).*

Tetrakis[4-(*N*-methyl-pyridinium-4-yl)phenyl]porphyrin tetraiodide (**11**) (105 mg, 0.070 mmol) was dissolved in water/ethanol (50:50) (5 mL). $KAuCl_4$ (107 mg, 0.283 mmol) was dissolved in water/ethanol (50:50) (5 mL) and added to the porphyrin solution. The mixture was refluxed overnight. After evaporation of ethanol and centrifugation, the aqueous phase was kept apart. Desalting of the porphyrin was performed by reverse phase chromatography on a Sep-Pak C18 cartridge (5 g) by elution

with ultrapure water followed by acetonitrile/water (30:70), containing 0.1% TFA. The collected fractions were evaporated to dryness and the product was taken in $CH_3OH/H_2O$ (50:50). Anion exchange was performed on a dowex 1x8-200 resin column (chloride form, 1 g). The product was precipitated by the addition of diethyl ether, filtered, and washed with ethanol. Yield: red orange solid, 25 mg, 20%. TLC ($SiO_2$, $CH_3CN/H_2O/KNO_3$sat., 8/1/1), Rf: 0.17. $^1$H NMR (400 MHz, MeOD, $\delta$ ppm): 9.50 (s, 8H, pyrrole), 9.11 (d, 8H, *J* = 7 Hz, pyridine), 8.78 (d, 8H, *J* = 7 Hz, pyridine), 8.63 – 8.59 (m, 16H, phenyl), 4.55 (s, 12H, methyl). $^{13}$C NMR (101 MHz, MeOD, $\delta$ ppm): 156.3, 146.5, 143.1, 137.6, 136.1, 135.9, 133.0, 128.0, 125.9, 123.129. $^{19}$F NMR (376 MHz, MeOD) no signal. HRMS-ES$^+$ (*m/z*): calcd. for $C_{68}H_{52}AuN_8$ 235.4796, found: 235.4793 $[M]^{5+}$. UV-vis ($H_2O$, $\lambda$ nm ($\varepsilon$ $m^{-1}$ $cm^{-1}$)): 410 (204 $10^3$), 523 (11 $10^3$).

*2.2.3. Preparation of meso-5,10,15-tris[4-(N-methylpyridinium-2-yl)phenyl]-20-[4-(N-methylpyridinium-4-yl)phenyl]porphyrinato gold(III) pentachloride (**5**)*

*2.2.3.1. Preparation of free base porphyrin meso-5,10,15-tris[4-(N-methyl-pyridinium-2-yl)phenyl]-20-[4-(N-methyl-pyridinium-4-yl)phenyl]porphyrin tetrachloride (**12**)*

Porphyrin **6** (40 mg, 0.043 mmol, 1 mol. equiv.) was placed in a Schlenk tube under argon with 4-pyridinylboronic acid (40 mg, 0.325 mmol, 5 mol. equiv.), $Pd(PPh_3)_4$ (5mg, 0.004 mmol) and $Cs_2CO_3$ (50 mg, 0.15 mmol). Then, 10 mL of anhydrous and degassed dioxane were added. The reaction mix was refluxed under argon overnight. The reaction was monitored by TLC and indicated full conversion of the starting material. The solvent was evaporated and DMF was added instead (10 mL). Iodomethane was added (1.5 mL) and the mixture was heated at 100 °C for 90 min. After *vacuum* distillation of DMF and iodomethane, the crude product was dissolved in $CH_3CN/H_2O/KNO_3$sat. (8/1/1) and purified by column chromatography using $CH_3CN/H_2O/KNO_3$sat. (8/1/1) as eluent. The second fraction was collected, evaporated, and ethanol was added for desalination. The ethanol phase was taken-off and evaporated. The crude product was dissolved in water. Precipitation of the porphyrin from saturated aqueous ammonium hexafluorophosphate (12 mol. equiv.) and from acetone with tetrabutylammonium chloride (12 mol. equiv.) afforded **12** [52]. Yield: red solid, 20 mg, 40%. TLC ($SiO_2$, $CH_3CN/H_2O/KNO_3$sat., 6/1/1), Rf: 0.31. $^1$H NMR (400 MHz, MeOD, $\delta$ ppm): 9.2 – 8.4 (broad signal, pyrrole), 9.22 (d, *J* = 6 Hz, 3H, py2), 9.08 (d, *J* = 7 Hz, 2H, py4), 8.82 (t, *J* = 7.5 Hz, 3H, py2), 8.76 (d, *J* = 7 Hz, 2H, py4), 8.59 – 8.56 (m, 8H, phe2, phe4), 8.53 (d, *J* = 6 Hz, 2H, phe4), 8.48 – 8.46 (m, 3H, py2), 8.28 – 8.24 (m, 3H, py2), 8.16 (d, *J* = 8 Hz, 2H, phe2), 8.15 (d, *J* = 8 Hz, 4H, phe2), 4.62 (s, 3H, $CH_3$-py2), 4.61 (s, 6H, $CH_3$-py2), 4.53 (s, 3H, $CH_3$-py4). $^{19}$F NMR (376 MHz, MeOD): no signal. HRMS-ES$^+$ (*m/z*): calcd. for $C_{68}H_{54}N_8$ 245.6112, found: 245.6120 $[M]^{4+}$. UV-vis ($H_2O$, $\lambda$ nm ($\varepsilon$ $m^{-1}$

$cm^{-1}$)): 416 (390 $10^3$), 517 (16 $10^3$), 554 (8.7 $10^3$), 581 (6.6 $10^3$), 635 (4.1 $10^3$). UV-vis (acidic $H_2O$, $\lambda$ nm): 440 (Soret Band), 649.

*2.2.3.2. Preparation of meso-5,10,15-tris[4-(N-methylpyridinium-2-yl)phenyl]-20-[4-(N-methylpyridinium-4-yl)phenyl]porphyrinato gold(III) pentachloride (**5**)*

Porphyrin **12** (30 mg, 0.026 mmol) was dissolved in $H_2O$/EtOH (50:50) with $KAuCl_4$ (25 mg, 0.066 mmol, 2.5 mol. equiv.) and NaOH (5 mol. equiv.). The metallation was monitored by UV-vis through the shift of the Soret band of the non-metallated porphyrin from 416 to 440 nm in acid medium. The reaction was refluxed until the metallation was completed. Desalting was performed using reverse phase Sep Pak C18 (5 g). Elution using $H_2O/CH_3CN$ (70:30) + 0.1% TFA afforded the porphyrin with TFA counter anions. Successive ammonium hexafluorophosphate and tetrabutylammonium chloride precipitation was performed to exchange TFA counter ions to chlorides. Yield: red orange solid, 6 mg, 17%. TLC ($SiO_2$, $CH_3CN/H_2O/KNO_3$sat., 6/1/1), Rf: 0.14. $^1$H NMR (400 MHz, MeOD, $\delta$ ppm): 9.59 (s, 4H, pyrrole), 9.57 (d, *J* = 5 Hz, 2H, pyrrole), 9.52 (d, *J* = 5 Hz, 2H, pyrrole), 9.24 (d, *J* = 6 Hz, 3H, pyr2), 9.12 (d, *J* = 6.5 Hz, 2H, py4), 8.85 – 8.82 (m, 3H, py2), 8.79 (d, *J* = 6.5 Hz, 2H, py4), 8.66 − 8.61 (m, 10H, phe2+phe4), 8.49 – 8.47 (m, 3H, py2), 8.30 – 8.24 (m, 9H, phe2+py2), 4.64 (s, 3H, $CH_3$-py2), 4.63 (s, 6H, $CH_3$-py2), 4.55 (s, 3H, $CH_3$-py4).$^{13}$C NMR (101 MHz, MeOD, $\delta$ppm): 156.4, 156.3, 147.7, 146.5, 143.1, 142.5, 137.7, 137.8, 137.7, 137.7, 136.0, 135.9, 135.5, 133.7, 133.2, 133.0, 131.1, 129.3, 128.1, 127.9, 127.3, 125.9, 123.2, 123.0. $^{19}$F NMR (376 MHz, MeOD): no signal. HRMS-ES$^+$ (*m/z*): calcd. for $C_{68}H_{52}AuN_8$ 235.4796, found: 235,4794 $[M]^{5+}$. UV-vis ($H_2O$ $\lambda$ nm ($\varepsilon$ $M^{-1}$ $cm^{-1}$)): 407 (330 $10^3$) (Soret band), 521 (15 $10^3$).

*2.3. G-quadruplex FRET melting experiments*

Four different labeled oligonucleotides were used in the FRET assay: F21T, F-HIV-21-T, F-HIV-321-T and F-HIV-32-T. The labeling consists of dual functionalization of oligonucleotides with the 5'-Fam and the 3'-Tamra fluorophore. F21T: 5'-Fam-d(GGGTTAGGGTTAGGGTTAGGG)-Tamra; F-HIV-21-T: 5'-Fam-d(TGGGCGGGACTGGGGAGTGGC)-Tamra; F-HIV-321-T: 5'-Fam-d(TGGCCTGGGCGGGACTGGG)-Tamra, F-HIV-32-T: 5'-Fam-d(AGGGAGGCGTGGCCTGGGCGGG)-Tamra. The sequence of the ds26 double-stranded competitor DNA is 5'-d(CAATCGGATCGAATTCGATCCGATTG).

The ligand-induced thermal stabilizations ($\Delta T_{1/2}$) were determined from FRET-melting experiments carried out in 96-well plates on a CFX96 real-time PCR equipment (Bio-Rad). After an initial stabilization at 20 °C for 10 min, the temperature was increased by a 0.5 °C step every minute until 99 °C. The melting experiments were performed at a final 0.2 µM strand concentration of oligonucleotide with 2 mol. equivalents of ligands relative to labeled oligonucleotide concentration. For FRET competition assays the ds26 duplex competitor was added to indicated concentrations (1, 4 and 10 µM)

corresponding to 5, 20 and 50 mol. equivalent with respect to the labeled oligonucleotide. The measurement buffer was 10 mM lithium cacodylate pH 7.2 buffer, 90 mM LiCl, 10 mM KCl for F21T and 10 mM lithium cacodylate pH 7.2 buffer, 100 mM KCl for HIV-oligonucleotides (F-HIV-21-T, F-HIV-321-T and F-HIV-32-T). Each experimental condition was assayed on three separate plates using triplicated wells. The data was analyzed with Prism.

*2.4. Molecular modeling*

*2.4.1. Docking experiments* The NMR structure of the parallel-stranded G-quadruplex of the HIV-1 genome was taken from the Brookhaven Protein Data Bank (PDB id. 2N4Y). The docked porphyrins of this study (**1** and **4**) were fully optimized before the docking stage with the PM7 Hamiltonian [53] implemented in the MOPAC 2016 quantum chemistry package [54]. The docking calculations were performed with the docking program Autodock, release 4.2.6 [55]. The Autodock graphical interface AutoDockTools [56] was used to keep polar hydrogens and add partial charges to the G4 nucleotide using the Kollman United charges. The search space was included in a box of 47 Å of side, centered on the guanine tetrad in interaction with the porphyrins (G5, G9, G16, G21) and with a grid spacing of 0.375 Å. The aromatic rings of porphyrins were allowed to rotate. Docking simulations were carried out using the Lamarckian Genetic Algorithm; the docking parameters were kept to their default values. For each calculation, ten poses ranked according to the scoring-function of Autodock were set.

*2.4.2. Quantum Chemical Calculations:* density functional theory calculations were performed with the Gaussian 09 suite [57]. Geometry optimizations were performed with the B3LYP functional [58] and the 6-31+G(d) basis set [59]. For gold atom, Ahlrichs' Def2TZVP basis set and polarization functions were used [60]. In order to limit the computational time, only the porphyrin and the four guanosines in contact with it (G5, G9, G16, G21) were considered. The guanosines were kept rigid while the geometry of the porphyrins was optimized. The interaction energies were calculated from the difference between the porphyrin-G4 system and the single entities (porphyrin and G4).

## 3. Results and discussion

### 3.1. Preparation of gold(III) porphyrins

The porphyrins used in the present work are shown in Scheme 1. The preparation of the gold(III) derivative of *meso*-5,10,15,20-tetrakis[4-(*N*-methyl-pyridinium-2-yl)phenyl]porphyrin (**1**) was previously published [39, 61].

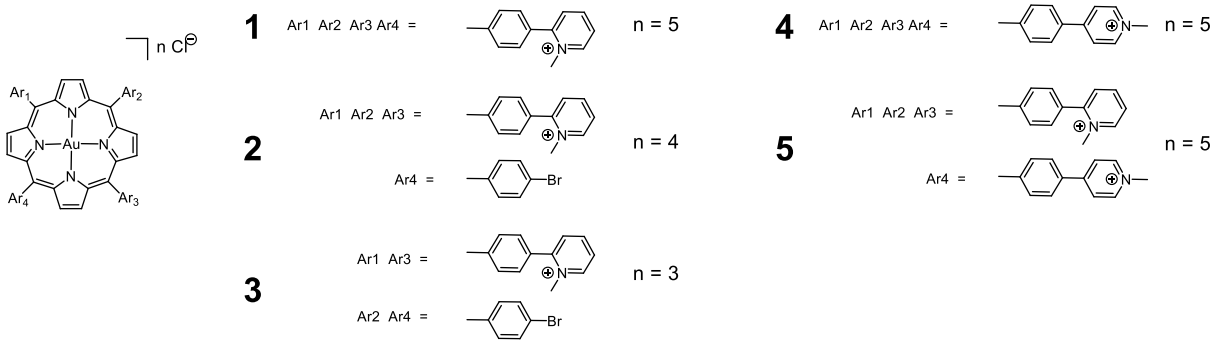


**Scheme 1**. Structures of the prepared gold(III) porphyrins

*Preparation of meso-5-(4-bromophenyl)-10,15,20-tris[4-(N-methyl-pyridinium-2-yl)phenyl]porphyrinato gold(III) tetrachloride (**2**) and meso-5,15-bis(4-bromophenyl)-10,20-bis[4-(N-methyl-pyridinium-2-yl)phenyl]porphyrinato gold(III) trichloride (**3**)*

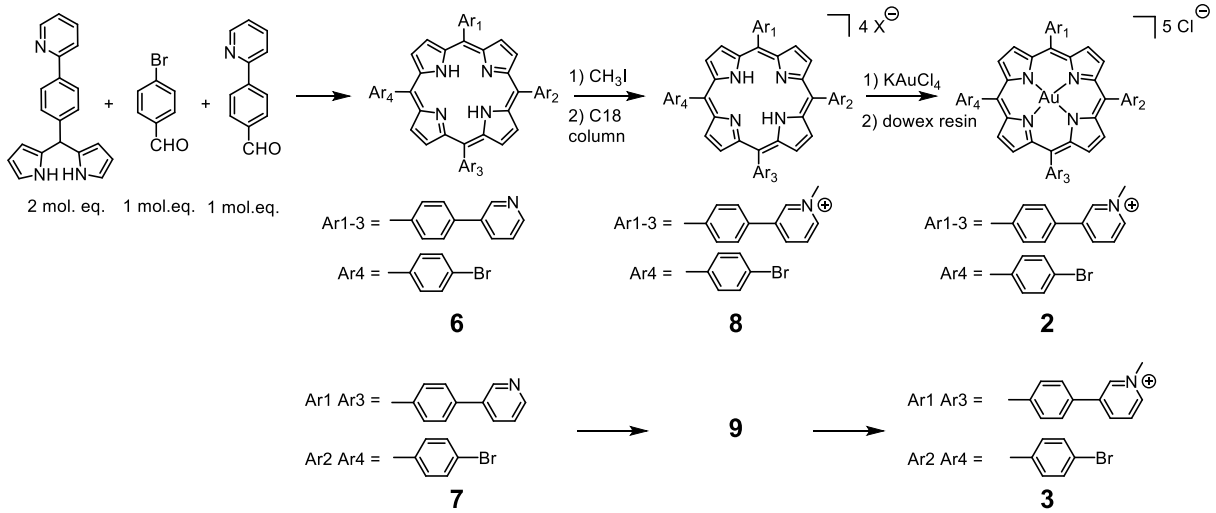


**Scheme 2**. Synthetic pathway of porphyrins **2** and **3**. X = trifluoroacetate.

We obtained the *meso*-5-(4-bromophenyl)-10,15,20-tris[4-(pyridin-2-yl)phenyl]porphyrin (**6**) and *meso*-5,15-bis(4-bromophenyl)-10,20-bis[4-(pyridin-2-yl)phenyl]porphyrin (**7**) starting from 4-bromobenzaldehyde, 4-(2-pyridinyl)benzaldehyde and 4-(2-pyridinyl)dipyrromethane (Scheme 2) [51], following the method described for the synthesis of other porphyrins in acidic medium [62, 63]. The mixture of porphyrins was separated by silica chromatography before the methylation step. Methylations with excess iodomethane of porphyrin **6** and porphyrin **7**, conducted separately, were not complete and were followed by a chromatography on $C_{18}$ reverse phase column to afford porphyrin **8** and **9**. Metallation by $KAuCl_4$ was also followed by a chromatography step, C18 reverse phase column for each porphyrin. Exchange of counter ions was performed on dowex 1x8 and afforded porphyrins **2** and **3** with chloride counter ions.

*Preparation of meso-tetrakis[4-(N-methylpyridinium-4-yl)phenyl]porphyrinato gold(III) pentachloride (**4**)*

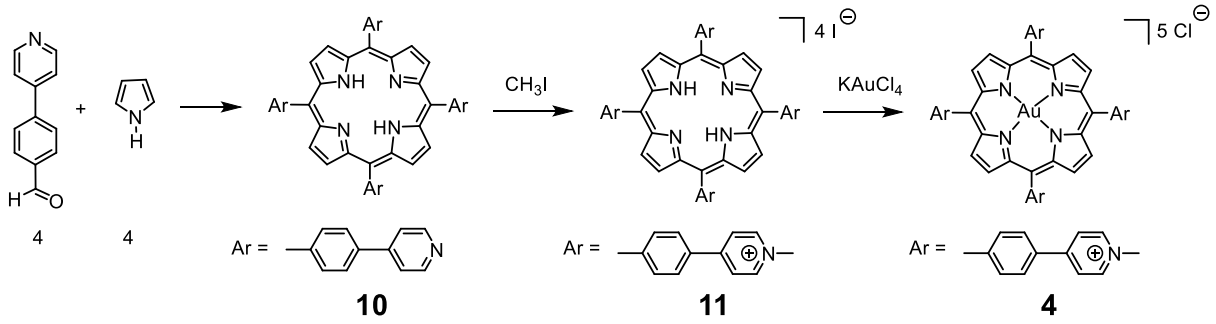


**Scheme 3**. Preparation of porphyrin **4**

The preparation of porphyrin **10** was adapted from a previously reported synthesis (Scheme 3) [33]. The methylation with iodomethane was complete and porphyrin **11** was obtained without intermediate chromatography. Metallation with $KAuCl_4$ was followed by a reverse phase chromatography to isolate the gold porphyrin. Exchange of counter ions, performed on dowex 1x8-200 resin, gave the chloride salt **4**. This compound is probably prone to self-stacking interactions in water since the measured epsilon value is lower than that generally measured for porphyrins bearing 4-(*N*-methyl-pyridinium-2-yl)phenyl substituents.

*Preparation of meso-5,10,15-tris[4-(N-methylpyridinium-2-yl)phenyl]-20-[4-(N-methylpyridinium-4-yl)phenyl]porphyrinato gold(III) pentachloride (**5**)*

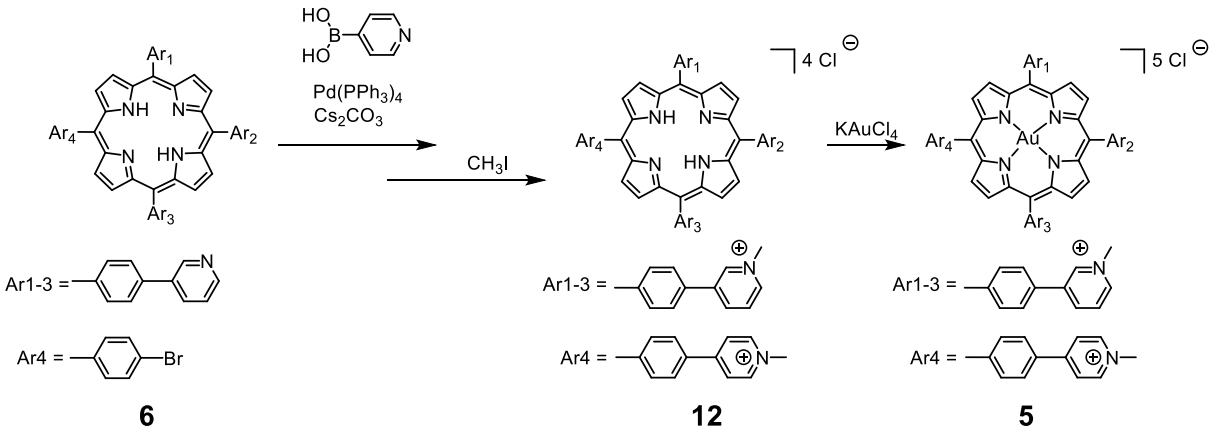


**Scheme 4**. Preparation of porphyrin **5**

Porphyrin **5** was prepared from *meso*-5-(4-bromophenyl)-10,15,20-tris[4-(pyridin-2-yl)phenyl]porphyrin **6** (Scheme 4). The Suzuki-Miyaura coupling reaction [64, 65] between **6** and 4-pyridylboronic acid, using *tetrakis*-(triphenylphosphine)palladium(0) as catalyst and cesium carbonate as a base led to intermediate porphyrin *meso*-5-(4-pyridin-4-yl)phenyl-10,15,20-tris[4-(pyridin-2-yl)phenyl]porphyrin (not isolated), which was further *N*-methylated into porphyrin **12**. The mixture of cationic methylated porphyrins was purified by silica chromatography with $CH_3CN/H_2O/KNO_3$sat. elution. Two successive precipitations of the porphyrin of interest (i) with ammonium hexafluorophosphate in water and (ii) tetrabutylammonium chloride in acetone [52] afforded porphyrin **12** with chloride counter ions. Metallation of **12** with $KAuCl_4$ followed by reverse phase chromatography afforded a porphyrin with trifluoroacetate counter ions that were exchanged to chloride counter ions by two successive precipitations to afford **5**.

Porphyrins **1** to **5** were soluble in water.

### 3.2. G-quadruplex DNA recognition by gold(III) cationic porphyrins

Porphyrin **1** was shown to be an excellent G-quadruplex ligand and showed promising antiviral properties [38, 39]. The porphyrin scaffold carries four positive charges, one for each *meso* substituent (Scheme 1). The insertion of an $Au^{3+}$ ion in the center of the porphyrin ring adds one positive charge to the complex and lowers the electron density on the porphyrin core. Thus, **1** is endowed with five positive charges, which grants a tight binding to G-quadruplex DNA through both π-stacking and

electrostatic interactions. As previously demonstrated, the bulky 4-(*N*-methyl-pryridinium-2-yl)phenyl substituents are suitable groups to allow selective recognition of G-quadruplex DNA versus duplex DNA [39], especially when compared to the smaller 4-*N*-methyl-pyridinium substituents of porphyrin TMPyP4. Having in mind the functionalization of porphyrin **1** to explore its antiviral mechanism of action, we explored some structural variations on the *meso* substituents and their consequences in terms of G-quadruplex recognition capacity. We report in the present work the removal of one and two positive charges from the *meso* substituents with porphyrin **2** and **3**, respectively. We also investigated the influence of the position of the positive charges with porphyrins **4** and **5**.

To evaluate the binding of gold(III) porphyrins to G-quadruplex DNA structures, we performed FRET melting assay [66, 67]. In this assay, the interaction of ligands with G4 structures is monitored by the increase of the half-melting temperature ($T_{1/2}$) of the G4-forming oligonucleotide in the presence of the ligand. The stabilization of the G4 structure formed by the oligonucleotide is expressed by the $\Delta T_{1/2}$ value resulting from the differences of half-melting temperatures measured with and without ligands. We first tested the binding of the gold porphyrins to the standard model of G-quadruplex DNA, the F21T oligonucleotide, modeling the telomeric sequence. The results are shown in Figure 1. One of the benchmark reference compounds in this assay is porphyrin TMPyP4. In $K^+$ conditions the addition of 2 mol. equivalents of TMPyP4 (0.4 µM) relative to F21T (0.2 µM) induced a $\Delta T_{1/2}$ of 18.5 °C [39]. In the same $K^+$ conditions, the addition of 2 mol. equivalents of **1** (0.4 µM) relative to F21T concentration (0.2 µM) induced a $\Delta T_{1/2}$ of 32.4 °C [39]. In the present work, porphyrin **1** stands for the reference compound. Comparison between **1** and porphyrins with a lower number of positive charges, namely, porphyrin **2** with one 4-bromophenyl substituent ($\Delta T_{1/2}$ F21T 2 eq. **2** = 8.7 °C ± 0.9) and porphyrin **3** with two 4-bromophenyl substituents ($\Delta T_{1/2}$ F21T 2 eq. **3** = 4.2 °C ± 0.9), shows that porphyrin **1** induced a significantly stronger thermal stabilization of F21T oligonucleotide, which indicates a much better ability to interact with G4-structures. The number of positive charges at the periphery of the porphyrin was previously reported to be of crucial importance in the targeting of G-quadruplex DNA [33, 46-49]. Therefore, to maintain a high affinity of the ligand for G-quadruplex DNA it does not seem judicious to plan modifications of porphyrin **1** without maintaining four positively charged substituents. The porphyrins bearing four positive arms, porphyrins **4** and **5**, proved able to stabilize F21T G-quadruplex in a more encouraging way. The symmetric porphyrin **4** with four 4-(*N*-methylpyridinium-4-yl)phenyl substituents ($\Delta T_{1/2}$ F21T 2 eq. **4** = 15.2 °C ± 0.9) and the porphyrin **5** with one 4-(*N*-methylpyridinium-4-yl)phenyl substituent ($\Delta T_{1/2}$ F21T 2 eq. **5** = 23.8 °C ± 0.9) did not reach the level of stabilization of porphyrin **1** but were fairly efficient. Thus, porphyrin **5** appeared to be the best porphyrin scaffold for functionalization at the unique 4-*N*-pyridine position. Comparison between the two symmetric porphyrins **1** and **4** showed that the location of the positive charge in porphyrin **4** seemed less suitable

for G4 DNA targeting. However, one cannot exclude that the apparent lower stabilization ability of **4** might be due to the higher propensity of this porphyrin to undergo self-stacking in solution. Indeed, compared to porphyrins **1** and **5**, the lower epsilon value of porphyrin **4** and the red shift of its Soret band suggest that the flat porphyrin **4** makes some stronger associations in solution, the nature of which remains to be studied. This phenomenon might be at the origin of a decreased concentration of monomers in solution. Modeling studies (see paragraph 3.3) did not provide a straightforward answer on the influence of the position of the positive charge (*N*-2 versus *N*-4) on the G4-porphyrin complex.

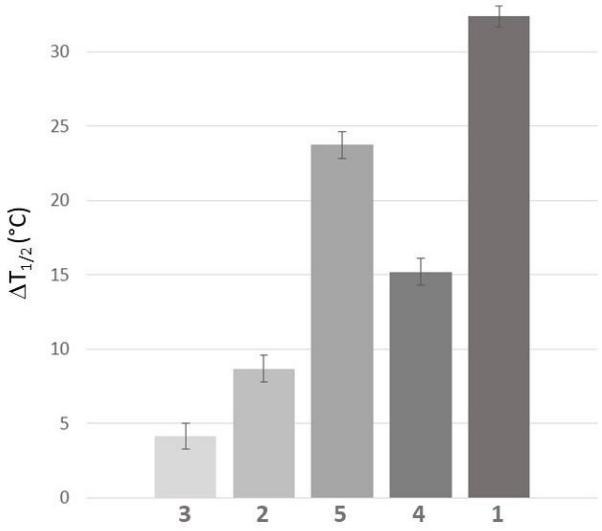


**Fig. 1**. Thermal stabilization of G4 structure by porphyrins **1** to **5**. Thermal stabilization of the F21T oligonucleotide measured by FRET melting assays. Porphyrin derivatives were added at 2 mol. equivalents (0.4 µM) with respect to F21T (0.2 µM) in 10 mM lithium cacodylate buffer pH 7.2, 90 mM LiCl and 10 mM KCl. The $\Delta T_{1/2}$ value indicates the difference of melting temperature induced by the ligand. For comparison, data of porphyrin **1** from [39].

The stabilization effect of a G4-ligand induces an increase in the melting temperature of the oligonucleotide ($\Delta T_{1/2}$). When a competitor DNA is added in the sample, the G4-ligand may bind to the competitor DNA. The consequent decrease in $\Delta T_{1/2}$ indicates the displacement of the G4-ligand from the G-quadruplex oligonucleotide to the competitor DNA. In the case of a selective G4-ligand, the $\Delta T_{1/2}$ is not affected by the presence of the competitor DNA. Therefore, the FRET melting assay is convenient for the evaluation of the binding properties of G4-ligands (stabilization and selectivity). It is particularly convenient for comparison purpose. The new gold(III) porphyrin derivatives **4**, and **5** stabilized G-quadruplex F21T DNA at 0.4 µM concentration, in the absence of competitor DNA, with $\Delta T_{1/2}$ of 15.2 and 23.8 °C, respectively (Figure 1). Figure 2 shows that the $\Delta T_{1/2}$ of F21T-porphyrin complex moderately decreased with increasing quantity of competitor DNA (5, 20 and 50 mol. equivalent with respect to F21T). In the case of **4** the $\Delta T_{1/2}$ decreased from 12.4, 8.3 and 4.0 °C in the presence of 5,

20 and 50 mol. equiv. of ds26, respectively. In the case of **5** the $\Delta T_{1/2}$ decreased from 20.2, 13.2 and 7.3 °C in the presence of 5, 20 and 50 mol. equiv. of ds26, respectively.

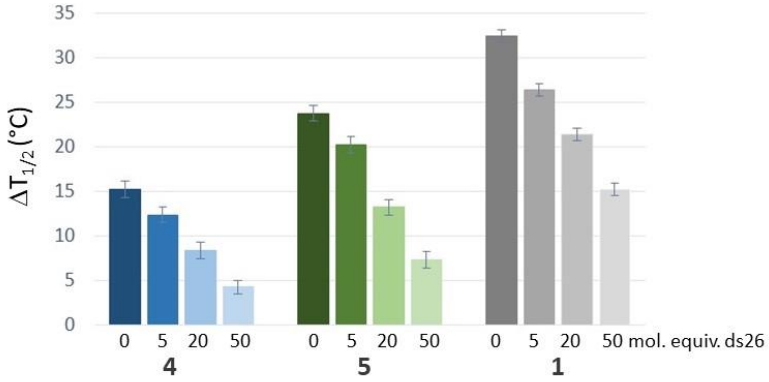


**Fig. 2**. Melting FRET competition assays. Thermal stabilization of G4 structure by porphyrins **1**, **4** and **5** in the presence of 5, 20 and 50 mol. equiv. of ds26 competitor (with respect to F21T). For competition assays competitor double-stranded DNA (ds26) (1, 4 and 10 µM) was added to the reaction containing porphyrins (0.4 µM) and F21T (0.2 µM). The $\Delta T_{1/2}$ value indicates the increase of melting temperature ($T_{1/2}$) of the F21T-porphyrin complex with respect to the F21T control in the absence of both ligand and competitor. For comparison, data of porphyrin **1** from [39].

The relatively stable $\Delta T_{1/2}$ of F21T-porphyrin complex in the presence of ds26 double-stranded DNA competitor is in favor of these three ligands being selective for G-quadruplex DNA.

The G4 stabilization capacity of the porphyrins was also assayed on three G-quadruplex forming sequences from the guanine-rich U3 region within the LTR promoter region of HIV-1 genome namely, F-HIV-21-T [41], F-HIV-321-T [40], and F-HIV-32-T [68] (Figure 3). Each DNA sequence topology is different. The structure of HIV-21 sequence showed a parallel folding while HIV-321 and HIV-32 fold in antiparallel and hybrid structure, respectively. The $\Delta T_{1/2}$ values corresponding to Figure 3 are reported in Table S1 (Supporting Information).

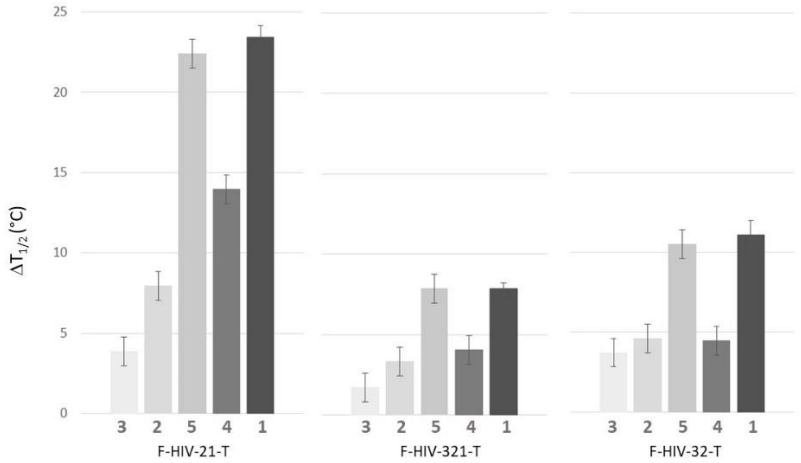


**Fig. 3**. Thermal stabilization of G4 structures by porphyrins **1** to **5**. Thermal stabilization of the F-HIV-21-T (parallel, left), F-HIV-321-T (anti-parallel, middle) and F-HIV-32-T (hybrid, right) oligonucleotides measured by FRET melting assays. Porphyrin derivatives were added at 2 mol. equivalents (0.4 µM) with respect to oligonucleotide (0.2 µM) in 10 mM lithium cacodylate buffer pH 7.2, 100 mM KCl. The $\Delta T_{1/2}$ value indicates the difference of melting temperature induced by the ligand.

The binding of the gold(III)porphyrins to the viral G-quadruplex models showed the same trend as seen with F21T sequence. The best ligand appeared to be porphyrin **5**, which showed on the HIV-1 G4s the same stabilization capacity as the standard compound porphyrin **1**. Porphyrin **4** showed intermediate behavior between porphyrin **5** and porphyrin **2**. In all cases, porphyrin **3** was the poorest G4 ligand. One can also note the higher binding of porphyrins to the parallel-folded G-quadruplex F-HIV-21-T.

### 3.3. Modeling studies of porphyrin/G-quadruplex complexes

We performed a molecular docking study to assess the potential role of the *N*-methyl position on the affinity of porphyrins **1** and **4** toward the G4s. Compounds **1** and **4** were docked on the parallel HIV-21 G-quadruplex (PDB id. 2N4Y) [41], using the Autodock 4 software [55]. The docking of porphyrin **1** (2-*N*-methyl pyridinium) only gave one cluster and that of porphyrin **4** (4-*N*-methyl pyridinium) three clusters, but with 7 poses in the first cluster. Figure 4 shows the docking results corresponding to the first cluster for **1** and **4**. The two poses are very similar and are superimposable. The gold center and the average plane of the G4 are separated by a distance of 4.1 Å. The pyridinium groups are positioned above the negatively charged phosphate groups for both of them.

It may be noted that the *N*-methyl pyridinium groups are slightly closer to the phosphate moieties in the case of **1** compared with **4**. The distance between the nitrogen and one of the oxygens of the phosphate groups ranges from about 2.6 to 3.4 Å for **1** and from about 3.0 to 4.0 Å for **4**. The calculated binding energies are -11.14 and -9.26 kcal/mol for **1** and **4**, respectively. The slightly better affinity of **1** might be explained by these shorter distances and therefore, a stronger interaction between the *N*-

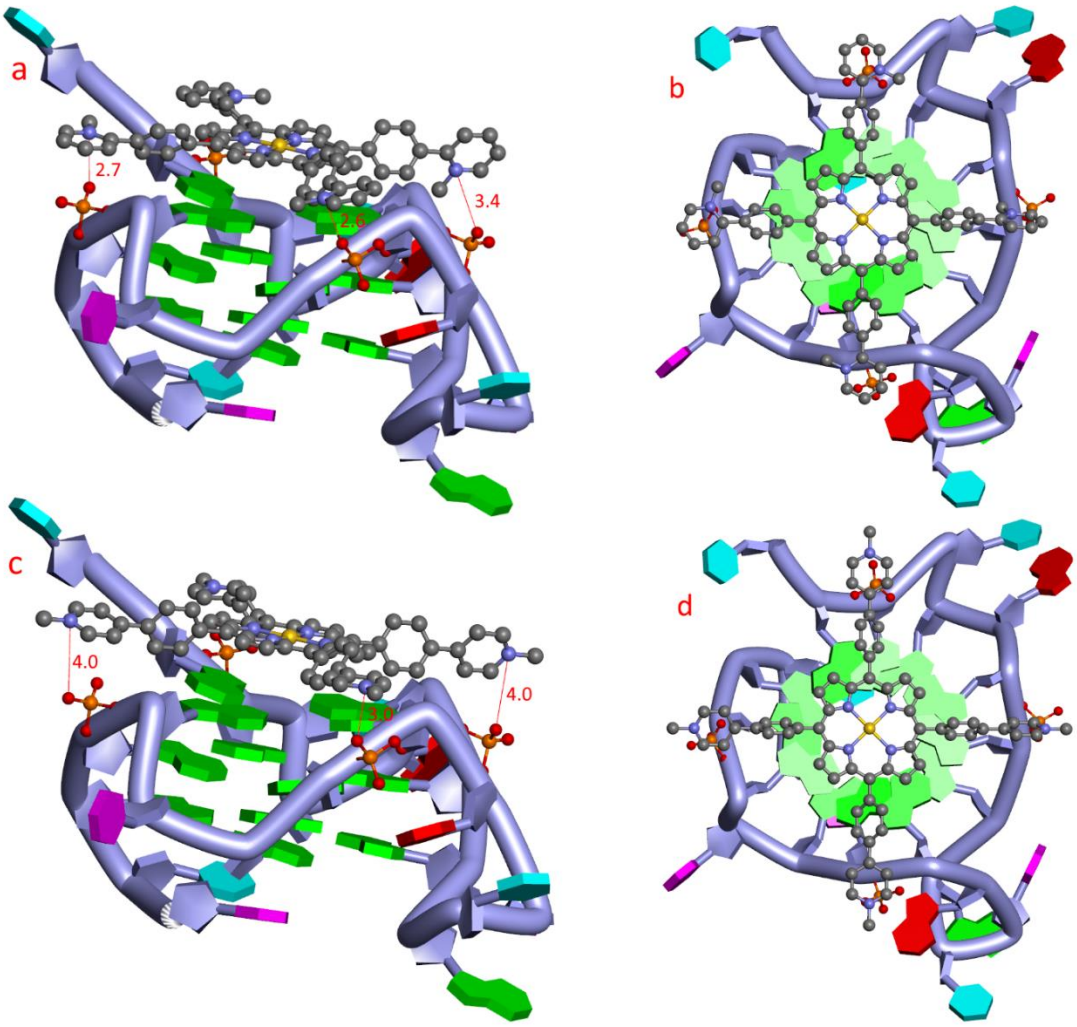


**Fig. 4**. The predicted binding modes of porphyrins **1** and **4** on the HIV-21 G-quadruplex (PDB id. 2N4Y). The two porphyrins are positioned such that the pyridinium groups are perfectly located above the phosphate groups (represented in ball and stick model). (a) and (b) side and front view of porphyrin **1;** (c) and (d) side and front view of porphyrin **4**. The distances between the *N*-methyl pyridinium and one oxygen belonging to the phosphate moieties are marked in red. Guanine cycles are colored green. For clarity, hydrogen atoms are omitted.

methyl pyridinium and the phosphate moieties, compared to **4**. However, the energy-gap of 1.88 kcal/mol is not high enough to explain the much better ability of **1** to interact with G4-structures. The affinity of the cationic porphyrins for the G4s is mainly under the dependence of electronic interactions. In order to take much better account of these electronic effects than a force-field does (as in Autodock), we performed quantum mechanical computations at the B3LYP/6-31+g(d) level (DEF2TZVP basis sets for gold atom) using the porphyrin conformations from the docking experiments as a starting point. The results of these calculations showed that both porphyrins exhibited an

equivalent interaction energy: we found a relative interaction energy of 1.40 kcal/mol in favor of compound **1**. However, this slight difference seems insufficient to explain the particular affinity of **1**.

Therefore, the propensity to aggregation of porphyrin **4** (decreasing the concentration of monomeric species) might be at the origin of the lower stabilization capacity of **4** in FRET melting experiments.

## 4. Conclusion

A structure/activity relationship study with porphyrins derived from porphyrin **1** was undertaken to better understand the key factors necessary for tight G-quadruplex binding. The synthesis of four new cationic gold(III) porphyrins (**2**-**5**) was reported. The preparation of mono-bromophenyl porphyrin **6** as a precursor of porphyrin **2** also allowed a Suzuki coupling reaction eventually affording porphyrin **5**. The best ligands must carry four cationic *meso*-substituents. Among them, porphyrin **5** proved to be as efficient as the antiviral porphyrin **1** in terms of affinity and selectivity for G-quadruplex DNA, therefore, we anticipate that porphyrin **5** will also have similar antiviral activity as observed for **1**. Hence, this porphyrin scaffold is a convenient basis for functionalization in view of deciphering the antiviral mechanism of action of porphyrin **1**.

## Declaration of competing interest

No potential conflict of interest was reported by the authors.

## Acknowledgement

This work was conducted with the support of the ANRS Maladies Infectieuses Émergentes – Agence autonome de l'Inserm (ECTZ103899). Dr. Dennis Gomez and Dr. Sébastien Britton, Institut de Pharmacolgie et de Biologie Structurale, CNRS IPBS, Toulouse, France, are acknowledged for technical assistance and helpful discussions.

## Appendix A. Supplementary data

Supplementary data to this article can be found online at https://doi.org/

**References**

[1] G.W. Collie, G.N. Parkinson, The application of DNA and RNA G-quadruplexes to therapeutic medicines, Chem. Soc. Rev., 40 (2011) 5867-5892.
[2] F.R. Winnerdy, A.T. Phan, Quadruplex structure and diversity, Annu. Rep. Med. Chem., 54 (2020) 45-73.
[3] R. Hänsel-Hertsch, M. Di Antonio, S. Balasubramanian, DNA G-quadruplexes in the human genome: detection, functions and therapeutic potential, Nat. Rev. Mol. Cell. Biol., 18 (2017) 279-284.
[4] D. Monchaud, Quadruplex detection in human cells, Annu. Rep. Med. Chem., 54 (2020) 133-160.
[5] N. Maizels, G4-associated human diseases, EMBO Rep., 16 (2015) 910-922.
[6] D. Varshney, J. Spiegel, K. Zyner, D. Tannahill, S. Balasubramanian, The regulation and functions of DNA and RNA G-quadruplexes, Nat. Rev. Mol. Cell. Biol., 21 (2020) 459-474.
[7] M.A. Al-Zeer, J. Kurreck, Deciphering the enigmatic biological functions of RNA guanine-quadruplex motifs in Human Cells, Biochemistry, 58 (2019) 305-311.
[8] D. Rhodes, H.J. Lipps, G-quadruplexes and their regulatory roles in biology, Nucleic Acids Res., 43 (2015) 8627-8637.
[9] R. Rigo, M. Palumbo, C. Sissi, G-quadruplexes in human promoters: a challenge for therapeutic applications, Biochim. Biophys. Acta Gen. Subj., 1861 (2017) 1399-1413.
[10] E. Ruggiero, S.N. Richter, G-quadruplexes and G-quadruplex ligands: targets and tools in antiviral therapy, Nucleic Acids Res., 46 (2018) 3270-3283.
[11] L.M. Harris, C.J. Merrick, G-quadruplexes in pathogens: a common route to virulence control?, PLoS Pathog., 11 (2015) e1004562.
[12] M. Métifiot, S. Amrane, S. Litvak, M.-L. Andreola, G-quadruplexes in viruses: function and potential therapeutic applications, Nucleic Acids Res., 42 (2014) 12352-12366.
[13] N. Saranathan, P. Vivekanandan, G-Quadruplexes: more than just a kink in microbial genomes, Trends Microbiol., 27 (2019) 148-163.
[14] S. Neidle, Quadruplex nucleic acids as novel therapeutic targets, J. Med. Chem., 59 (2016) 5987-6011.
[15] Z.Y. Sun, X.N. Wang, S.Q. Cheng, X.X. Su, T.M. Ou, Developing novel G-quadruplex ligands: from interaction with nucleic acids to interfering with nucleic acid–protein interaction, Molecules, 24 (2019) 396.
[16] R. Simone, P. Fratta, S. Neidle, G.N. Parkinson, A.M. Isaacs, G-quadruplexes: emerging roles in neurodegenerative diseases and the non-coding transcriptome, FEBS Lett., 589 (2015) 1653-1668.
[17] J. Dai, Z.Q. Liu, X.Q. Wang, J. Lin, P.F. Yao, S.L. Huang, T.M. Ou, J.H. Tan, D. Li, L.Q. Gu, Z.S. Huang, Discovery of small molecules for up-regulating the translation of antiamyloidogenic secretase, a disintegrin and metalloproteinase 10 (ADAM10), by binding to the G-Quadruplex-forming sequence in the 5' untranslated region (UTR) of its mRNA, J. Med. Chem., 58 (2015) 3875-3891.
[18] S. Asamitsu, T. Bando, H. Sugiyama, Ligand design to acquire specificity to intended G-quadruplex structures, Chem. Eur. J., 25 (2019) 417-430.
[19] D. Monchaud, M.P. Teulade-Fichou, A hitchhiker's guide to G-quadruplex ligands, Org. Biomol. Chem., 6 (2008) 627-636.
[20] D. Monchaud, A. Granzhan, N. Saettel, A. Guedin, J.-L. Mergny, M.-P. Teulade-Fichou, "One ring to bind them all"-part I: the efficiency of the macrocyclic scaffold for G-quadruplex DNA recognition, J. Nucleic Acids (2010) 525862,.
[21] A. Granzhan, D. Monchaud, N. Saettel, A. Guedin, J.-L. Mergny, M.-P. Teulade-Fichou, "One ring to bind them all"-Part II: identification of promising G-quadruplex ligands by screening of cyclophane-type macrocycles, J. Nucleic Acids (2010) 460561.
[22] R. Vilar, Nucleic Acid quadruplexes and metallo-drugs, Met. Ions Life Sci., 18 (2018) 325-349.
[23] Q. Cao, Y. Li, E. Freisinger, P.Z. Qin, R.K.O. Sigel, Z.W. Mao, G-quadruplex DNA targeted metal complexes acting as potential anticancer drugs, Inorg Chem Front, 4 (2017) 10-32.

[24] P. Murat, Y. Singh, E. Defrancq, Methods for investigating G-quadruplex DNA/ligand interactions, Chem. Soc. Rev., 40 (2011) 5293-5307.
[25] E. Ruggiero, S.N. Richter, Viral G-quadruplexes: new frontiers in virus pathogenesis and antiviral therapy, Annu. Rep. Med. Chem., 54 (2020) 101-131.
[26] C. Jaubert, A. Bedrat, L. Bartolucci, C. Di Primo, M. Ventura, J.-L. Mergny, S. Amrane, M.-L. Andreola, RNA synthesis is modulated by G-quadruplex formation in hepatitis C virus negative RNA strand, Sci. Rep., 8 (2018) 8120.
[27] A. Madireddy, P. Purushothaman, C.P. Loosbroock, E.S. Robertson, C.L. Schildkraut, S.C. Verma, G-quadruplex-interacting compounds alter latent DNA replication and episomal persistence of KSHV, Nucleic Acids Res., 44 (2016) 3675-3694.
[28] A. Granzhan, R.P. Martins, R. Fåhraeus, M. Blondel, M.P. Teulade-Fichou, Quadruplex-interacting compounds for regulating the translation of the Epstein–Barr virus nuclear antigen 1 (EBNA1) mRNA: a new strategy to prevent and treat EBV-related cancers, Annu. Rep. Med. Chem., 54 (2020) 243-286.
[29] A.T. Phan, V. Kuryavyi, H.Y. Gaw, D.J. Patel, Small-molecule interaction with a five-guanine-tract G-quadruplex structure from the human MYC promoter, Nat. Chem. Biol., 1 (2005) 167-173.
[30] J.M. Nicoludis, S.T. Miller, P.D. Jeffrey, S.P. Barrett, P.R. Rablen, T.J. Lawton, L.A. Yatsunyk, Optimized end-stacking provides specificity of N-methyl mesoporphyrin IX for human telomeric G-quadruplex DNA, J. Am. Chem. Soc., 134 (2012) 20446-20456.
[31] R.T. Wheelhouse, D. Sun, H. Han, F.X. Han, L.H. Hurley, Cationic porphyrins as telomerase inhibitors: the interaction of tetra-(N-methyl-4-pyridyl)porphine with quadruplex DNA, J. Am. Chem. Soc., 120 (1998) 3261-3262.
[32] G. Pratviel, Porphyrins in complex with DNA: modes of interaction and oxidation reactions, Coord. Chem. Rev., 308 (2016) 460-477.
[33] S.F. Jin, P. Zhao, L.C. Xu, M. Zheng, J.Z. Lu, P.L. Zhao, Q.L. Su, H.X. Chen, D.T. Tang, J. Chen, J.Q. Lin, Synthesis, G-quadruplexes DNA binding, and photocytotoxicity of novel cationic expanded porphyrins, Bioorg. Chem., 60 (2015) 110-117.
[34] X.Y. Sun, P. Zhao, S.F. Jin, M.C. Liu, X.H. Wang, Y.M. Huang, Z.F. Cheng, S.Q. Yan, Y.Y. Li, Y.Q. Chen, Y.M. Zhong, Shedding lights on the flexible-armed porphyrins: human telomeric G4 DNA interaction and cell photocytotoxicity research, J. Photochem. Photobiol. B, 173 (2017) 606-617.
[35] N.C. Sabharwal, J. Chen, J.H.J. Lee, C.M.A. Gangemi, A. D'Urso, L.A. Yatsunyk, Interactions between spermine-derivatized tentacle porphyrins and the human telomeric DNA G-quadruplex, Int. J. Mol. Sci., 19 (2018) 3686.
[36] Y.F. Huo, L.N. Zhu, X.Y. Li, G.M. Han, D.M. Kong, Water soluble cationic porphyrin showing pH-dependent optical responses to G-quadruplexes: applications in pH-sensing and DNA logic gate, Sensors Actuat. B-Chem., 237 (2016) 179-189.
[37] R. Zhang, M. Cheng, L.M. Zhang, L.N. Zhu, D.M. Kong, Asymmetric cationic porphyrin as a new G-quadruplex probe with wash-free cancer-targeted imaging ability under acidic microenvironments, ACS Appl. Mater. Interfaces, 10 (2018) 13350-13360.
[38] S. Amrane, M.-A. Andreola, G. Pratviel, J.-L. Mergny, Derivatives of Porphyrins, Their Process of Preparation and Their Use for Treating Viral Infections, US20200223858A1, July 16, 2020.
[39] A. Pipier, A. De Rache, C. Modeste, S. Amrane, E. Mothes-Martin, J.-L. Stigliani, P. Calsou, J.-L. Mergny, G. Pratviel, D. Gomez, G-Quadruplex binding optimization by gold(III) insertion into the center of a porphyrin, Dalton Trans., 48 (2019) 6091-6099.
[40] S. Amrane, A. Kerkour, A. Bedrat, B. Vialet, M.-L. Andreola, J.-L. Mergny, Topology of a DNA G-quadruplex structure formed in the HIV-1 promoter: a potential target for anti-HIV drug development, J. Am. Chem. Soc., 136 (2014) 5249-5252.
[41] B. De Nicola, C.J. Lech, B. Heddi, S. Regmi, I. Frasson, R. Perrone, S.N. Richter, A.T. Phan, Structure and possible function of a G-quadruplex in the long terminal repeat of the proviral HIV-1 genome, Nucleic Acids Res., 44 (2016) 6442-6451.
[42] D. Piekna-Przybylska, M.A. Sullivan, G. Sharma, R.A. Bambara, U3 region in the HIV-1 genome adopts a G-quadruplex structure in its RNA and DNA sequence, Biochemistry, 53 (2014) 2581-2593.

[43] W. Shen, L. Gao, M. Balakrishnan, R.A. Bambara, A recombination hot spot in HIV-1 contains guanosine runs that can form a G-quartet structure and promote strand transfer in vitro, J. Biol. Chem., 284 (2009) 33883-33893.
[44] D. Piekna-Przybylska, G. Sharma, R.A. Bambara, Mechanism of HIV-1 RNA dimerization in the central region of the genome and significance for viral evolution, J. Biol. Chem., 288 (2013) 24140-24150.
[45] S. Lyonnais, R.J. Gorelick, J.-L. Mergny, E. Le Cam, G. Mirambeau, G-quartets direct assembly of HIV-1 nucleocapsid protein along single-stranded DNA, Nucleic Acids Res., 31 (2003) 5754-5763.
[46] T.L. Ruan, S.J. Davis, B.M. Powell, C.P. Harbeck, J. Habdas, P. Habdas, L.A. Yatsunyk, Lowering the overall charge on TMPyP4 improves its selectivity for G-quadruplex DNA, Biochimie, 132 (2017) 121-130.
[47] G.B. Rowland, K. Barnett, J.I. DuPont, G. Akurathi, V.H. Le, E.A. Lewis, The effect of pyridyl substituents on the thermodynamics of porphyrin binding to G-quadruplex DNA, Bioorgan Med Chem, 21 (2013) 7515-7522.
[48] D.F. Shi, R.T. Wheelhouse, D. Sun, L.H. Hurley, Quadruplex-interactive agents as telomerase inhibitors: synthesis of porphyrins and structure-activity relationship for the inhibition of telomerase, J. Med. Chem., 44 (2001) 4509-4523.
[49] C.I. Ramos, J.P. Tome, M.G. Santana-Marques, Charge and substituent effects on the stability of porphyrin/G-quadruplex adducts, J. Mass Spectrom., 47 (2012) 173-179.
[50] F. Caporaletti, J. Rubio-Magnieto, M. Lo, J.-F. Longevial, C. Rose, S. Clément, A. van der Lee, M. Surin, S. Richeter, Design of metalloporphyrins fused to imidazolium rings for binding DNA G-quadruplexes, J. Porphyr. Phthalocya., 24 (2020) 342-349.
[51] N. Malatesti, K. Smith, H. Savoie, J. Greenman, R.W. Boyle, Synthesis and in vitro investigation of cationic 5,15-diphenyl porphyrin-monoclonal antibody conjugates as targeted photodynamic sensitisers, Int. J. Oncol., 28 (2006) 1561-1569.
[52] I. Batinic-Haberle, L. Benov, I. Spasojevic, I. Fridovich, The ortho effect makes manganese(III) meso-tetrakis(N-methylpyridinium-2-yl)porphyrin a powerful and potentially useful superoxide dismutase mimic, J. Biol. Chem., 273 (1998) 24521-24528.
[53] J.J. Stewart, Optimization of parameters for semiempirical methods VI: more modifications to the NDDO approximations and re-optimization of parameters, J. Mol. Model., 19 (2013) 1-32.
[54] MOPAC2016, Version: 20.079L, James J. P. Stewart, Stewart Computational Chemistry, Colorado Springs, CO, http://OpenMOPAC.net.
[55] R. Huey, G.M. Morris, A.J. Olson, D.S. Goodsell, A semiempirical free energy force field with charge-based desolvation, J. Comput. Chem., 28 (2007) 1145-1152.
[56] G.M. Morris, R. Huey, W. Lindstrom, M.F. Sanner, R.K. Belew, D.S. Goodsell, A.J. Olson, AutoDock4 and AutoDockTools4: automated docking with selective receptor flexibility, J. Comput. Chem., 30 (2009) 2785-2791.
[57] M.J. Frisch, G.W. Trucks, H.B. Schlegel, G.E. Scuseria, M.A. Robb, J.R. Cheeseman, G. Scalmani, V. Barone, B. Mennucci, G.A. Petersson, H. Nakatsuji, M. Caricato, X. Li, H.P. Hratchian, A.F. Izmaylov, J. Bloino, G. Zheng, J.L. Sonnenberg, M. Hada, M. Ehara, K. Toyota, R. Fukuda, J. Hasegawa, M. Ishida, T. Nakajima, Y. Honda, O. Kitao, H. Nakai, T. Vreven, J.A. Montgomery, Jr., J.E. Peralta, F. Ogliaro, M. Bearpark, J.J. Heyd, E. Brothers, K.N. Kudin, V.N. Staroverov, T. Keith, R. Kobayashi, J. Normand, K. Raghavachari, A. Rendell, J.C. Burant, S.S. Iyengar, J. Tomasi, M. Cossi, N. Rega, J.M. Millam, M. Klene, J.E. Knox, J.B. Cross, V. Bakken, C. Adamo, J. Jaramillo, R. Gomperts, R.E. Stratmann, O. Yazyev, A.J. Austin, R. Cammi, C. Pomelli, J.W. Ochterski, R.L. Martin, K. Morokuma, V.G. Zakrzewski, G.A. Voth, P. Salvador, J.J. Dannenberg, S. Dapprich, A.D. Daniels, O. Farkas, J.B. Foresman, J.V. Ortiz, J. Cioslowski, and D.J. Fox. Gaussian Inc., Wallingford CT, 2013.
[58] A.D. Becke, Density-functional thermochemistry. III. The role of exact exchange, J. Chem. Phys., 98 (1993) 5648.
[59] R. Ditchfield, W.J. Hehre, J.A. Pople, Self-Consistent Molecular-Orbital Methods. IX. An Extended Gaussian-Type Basis for Molecular-Orbital Studies of Organic Molecules, J. Chem. Phys., 54 (1971) 724.

[60] A. Schäfer, C. Huber, R. Ahlrichs, Fully optimized contracted Gaussian basis sets of triple zeta valence quality for atoms Li to Kr, J. Chem. Phys., 100 (1994) 5829.
[61] C. Romera, L. Sabater, A. Garofalo, I.M. Dixon, G. Pratviel, Interaction of cationic nickel and manganese porphyrins with the minor groove of DNA, Inorg. Chem., 49 (2010) 8558-8567.
[62] A.D. Adler, F.R. Longo, J.D. Finarelli, J. Goldmacher, J. Assour, L. Korsakoff, A simplified synthesis for meso-tetraphenylporphin, J. Org. Chem., 32 (1967) 476.
[63] C. Casas, C.J. Lacey, B. Meunier, Preparation of hybrid "DNA cleaver-oligonucleotide" molecules based on a metallotris(methylpyridiniumyl)porphyrin motif, Bioconjug. Chem., 4 (1993) 366-371.
[64] J.P. Tremblay-Morin, H. Ali, J.E. van Lier, Palladium catalyzed coupling reactions of cationic porphyrins with organoboranes (Suzuki) and alkenes (Heck), Tetrahedron Lett., 47 (2006) 3043-3046.
[65] M. Haeubl, S. Schuerz, B. Svejda, L.M. Reith, B. Gruber, R. Pfragner, W. Schoefberger, Asymmetrically substituted cationic indole- and fluorene porphyrins inhibit tumor proliferation in small intestinal neuroendocrine tumors and medullary thyroid carcinomas, Eur. J. Med. Chem., 45 (2010) 760-773.
[66] J.-L. Mergny, J.-C. Maurizot, Fluorescence resonance energy transfer as a probe for G-quartet formation by a telomeric repeat, ChemBioChem, 2 (2001) 124-132.
[67] A. De Cian, L. Guittat, M. Kaiser, B. Sacca, S. Amrane, A. Bourdoncle, P. Alberti, M.-P. Teulade-Fichou, L. Lacroix, J.-L. Mergny, Fluorescence-based melting assays for studying quadruplex ligands, Methods, 42 (2007) 183-195.
[68] M. Arévalo-Ruiz, S. Amrane, F. Rosu, E. Belmonte-Reche, P. Penalver, J.-L. Mergny, J.C. Morales, Symmetric and dissymmetric carbohydrate-phenyl ditriazole derivatives as DNA G-quadruplex ligands: synthesis, biophysical studies and antiproliferative activity, Bioorg. Chem., 99 (2020) 103786.